DOI: 10.1002/ejic.200600068

A Two-Step Spin Transition and Order–Disorder Phenomena in the Mononuclear Compound [Fe(Hpy-DAPP)]$(BF_4)_2$

Galina S. Matouzenko,*[a] Dominique Luneau,[b] Gábor Molnár,[c] Nawell Ould-Moussa,[c] Samir Zein,[a] Serguei A. Borshch,[a] Azzedine Bousseksou,[c] and Frédéric Averseng[a]

Keywords: Density functional calculations / Iron / Magnetic properties / Mössbauer spectroscopy / N ligands / Spin crossover

This paper reports the synthesis and detailed characterization of the mononuclear complex $[Fe^{II}(Hpy\text{-}DAPP)](BF_4)_2$ (Hpy-DAPP = {bis[*N*-(2-pyridylmethyl)-3-aminopropyl](2-pyridylmethyl)amine}), which manifests a two-step spin crossover accompanied by an ordering and a conformational transition in the ligand. The magnetic susceptibility measurements and Mössbauer spectra reveal that the two steps of the spin transition are separated by an inflexion point at about 130 K at which 50 % of the complex undergoes a spin conversion. The high-temperature step centered at 181 K is gradual, whereas the low-temperature one displays a thermal hysteresis with two transition temperatures ($T_{c\downarrow}$ = 119 and $T_{c\uparrow}$ = 123 K). The single-crystal X-ray structure has been determined for the HS (298 K) and LS (90 K) forms, as well as for the mixed form with an HS:LS ratio of 1:1 (130 K). The structural studies show that the crystal lattice contains a single Fe^{II} crystallographic site over the whole temperature range. At room temperature, the most important peculiarity of the HS complex structure is the disorder of the N3 amino aliphatic atom, which is in the first coordination sphere of Fe^{II}, over two positions. The strong involvement of the N3 atoms in H-bonding with two neighboring counterions is considered as a possible origin of this disorder. At 130 K, the disorder is increased by the distribution of the N1 and C9 atoms over two positions, leading to the conformational disorder (*chair* and *twist-boat* conformations with a 1:1 ratio) in the six-membered N2C7C8C9N1Fe chelate cycle. At 90 K, the disorder in the positions of the N1, N3, and C9 atoms disappears and the N2C7C8C9N1Fe metallacycle adopts a unique *twist-boat* conformation. The results of structural studies suggest that the two-step spin-transition behavior of the complex $[Fe(Hpy\text{-}DAPP)](BF_4)_2$ is induced by two different geometries of the $[FeN_6]$ coordination core generated by the disorder in the ligand. The HS → LS transition is also associated with the conformational change in the chelate cycle. Both crystallographic data analysis and electronic structure calculations allow us to relate the disordered geometries of the $[FeN_6]$ coordination core to their HS and LS character.

Introduction

The phenomenon of spin transition between low-spin (LS) and high-spin (HS) electronic states[1] is an important area in iron(II) coordination chemistry. Its theoretical and experimental aspects, as well as its potential applications, give rise to a permanent interest in this phenomenon. The bi-stable behavior (HS, $S = 2$, $^5T_2 \leftrightarrow$ LS, $S = 0$, $^1A_1$) underlies the design of new molecular materials for technological applications[1b,1d,2] and can be induced by a variation of temperature, pressure, light irradiation, or by application of a magnetic field. The potential applications of spin-crossover systems for information storage require an abrupt spin transition with a relatively large thermal hysteresis centered near to ambient temperature. Currently, two approaches are employed to design new cooperative spin-crossover compounds, namely supramolecular and polymeric approaches.[3] The use of new polydentate ligands containing nitrogen donor atoms with different chemical functions, which generate an intermediate ligand field that favors spin-state interconversion, is one of the possible synthetic strategies for engineering spin transition systems. However, the ligand-field splitting is not the only factor that determines the existence and character of a spin transition. The interplay of the spin pairing energy and the ligand-field strength is very sensitive to small structural perturbations in the metal environment, which may result from the existence of sterically demanding ligands and/or from minor crystal-packing changes associated with the nature of the counterions, or even the presence of a solvent of crystallization. As has been noted,[1i] even more subtle changes, such as the number of chelate rings and/or the replacement of five- with six-membered cycles, can also affect the spin state of the

[a] Laboratoire de Chimie (UMR CNRS and ENS-Lyon n° 5182), École Normale Supérieure de Lyon,
46, allée d'Italie, 69364 Lyon cedex 07, France
E-mail: Galina.Matouzenko@ens-lyon.fr
[b] Université Claude Bernard Lyon-1, Laboratoire des Multimatériaux et Interfaces (UMR CNRS n° 5615),
69622 Villeurbanne cedex, France
[c] Laboratoire de Chimie de Coordination (UPR CNRS n° 8241),
205, route de Narbonne, 31077 Toulouse cedex, France
Supporting information for this article is available on the WWW under http://www.eurjic.org or from the author.

resulting iron(II) complex. In this context, polydentate ligands that are capable of generating one or more flexible six-membered metallocycles upon coordination with Fe^{II} are of special interest. In this case, a high flexibility of the coordination sphere of a complex can manifest itself in different ways, one of which is the yield of several reaction products. For example, the enlargement of just one of three chelate cycles from five-membered in $[Fe(DPEA)(NCS)_2]$[4a] [DPEA = (2-aminoethyl)bis(2-pyridylmethyl)amine] to six-membered in $[Fe(DPPA)(NCS)_2]$[4b] [DPPA = (3-aminopropyl)bis(2-pyridylmethyl)amine] has allowed the isolation of four species with the DPPA ligand (three of them with the spin change), namely three polymorphic modifications and one solvated complex, instead of just one complex with DPEA. Another situation arises due to the conformational freedom of six-membered chelate cycles.[5] Recently, a new cooperative spin-crossover compound $[Fe(DAPP)(abpt)](ClO_4)_2$ [DAPP = bis(3-aminopropyl)(2-pyridylmethyl)-amine; abpt = 4-amino-3,5-bis(pyridin-2-yl)-1,2,4-triazole], which displays simultaneous spin change and two order–disorder transitions (in the DAPP ligand and the counterion), has been reported.[6] At high temperatures, the disorder over two positions was observed for one carbon atom in the six-membered metallacycle, which is in a *half-boat* conformation. This peculiarity, i.e. the thermal ordering of the ligand directly coordinated to the metal, was documented for spin-crossover systems for the first time. The order–disorder phenomena and the spin transition in $[Fe(DAPP)(abpt)](ClO_4)_2$ were found to be interrelated. Both tuning of the ligand-field strength by the DAPP ligand and reinforcement of the cooperative interactions due to the thermal ordering in the perchlorate ions were proposed as initiators of the spin transition.

Following our studies on the role of metallocycle size on the spin-transition process, a new complex $[Fe(Hpy-DAPP)](BF_4)_2$ (Hpy-DAPP = {bis[*N*-(2-pyridylmethyl)-3-aminopropyl](2-pyridylmethyl)amine}) has been synthesized. The hexadentate Hpy-DAPP ligand (Scheme 1) was prepared starting from tetradentate DAPP. The modification of the DAPP ligand was motivated by its ability to form disordered six-membered chelate cycles upon coordination with Fe^{II}. The magnetic susceptibility measurements and Mössbauer spectra of the title compound display a two-step spin transition with thermal hysteresis in the low-temperature step. The single-crystal X-ray structure was determined for the HS (298 K) and LS (90 K) forms, as well as for the mixed form with an HS:LS ratio of 1:1 (130 K). The results of our experimental and theoretical studies suggest that $[Fe(Hpy-DAPP)](BF_4)_2$ can be considered as the first mononuclear complex with a unique Fe^{II} crystallographic site for which the two-step spin transition occurs within the same space group and is accompanied by a ligand ordering in conjugation with a conformational transition.

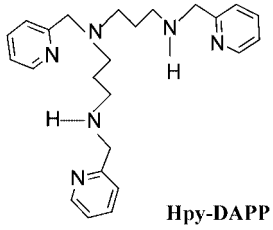

Scheme 1. Representation of the Hpy-DAPP ligand.

Results

Magnetic Susceptibility Data

Magnetic susceptibility measurements were carried out on two different batches of freshly prepared samples of $[Fe(Hpy-DAPP)](BF_4)_2$ and also on some thermally cycled samples. Within the experimental precision, the magnetic susceptibility of these samples was the same at each temperature. Variable-temperature magnetic susceptibility data were measured in both cooling and warming modes in the range 15–290 K. The magnetic properties of the complex (Figure 1) display the HS ↔ LS transition. At 290 K, the magnitude of $\chi_M T$, where χ_M is the molar magnetic susceptibility, is 3.56 $cm^3 mol^{-1} K$ (μ_{eff} = 5.34 μ_B) and corresponds to a quintet spin state. This value remains fairly constant with decreasing temperature until 230 K and then gradually decreases upon cooling to 1.78 $cm^3 mol^{-1} K$ at 130 K. Below 130 K, the $\chi_M T$ value descends more steeply to reach 0.53 $cm^3 mol^{-1} K$ at 90 K, and then it slowly decreases to 0.40 $cm^3 mol^{-1} K$ at 15 K. This weak paramagnetism may be related to a residual amount (about 10%) of the HS fraction. The presence of a residual paramagnetic HS fraction at low temperature was confirmed by Mössbauer spectroscopy (vide infra). The shape of the susceptibility curve reveals that the spin transition takes place in two steps, which are separated by an inflexion point at about 130 K at which 50% of the complex has undergone a thermal spin conversion. The gradual high-temperature step is centered at 181 K. The low-temperature step displays a thermal hysteresis. The observed transition temperatures are $T_{c\downarrow}$ = 119 and $T_{c\uparrow}$ = 123 K in the cooling and warming modes, respectively.

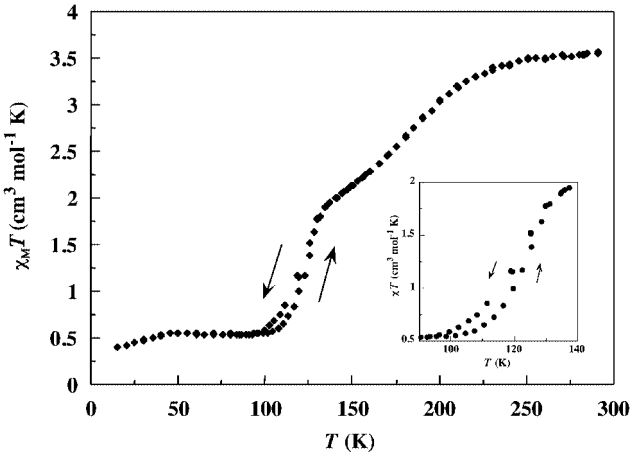

Figure 1. Thermal variation of $\chi_M T$ for $[Fe(Hpy-DAPP)](BF_4)_2$.

Description of the Structure

The crystal structure of [Fe(Hpy-DAPP)]$(BF_4)_2$ was determined at 298, 130, and 90 K for the HS, mixed-spin states, and predominantly LS form, respectively. No change in the space group was observed at these three temperatures. All structures belong to the monoclinic $P2_1/c$ group with $Z = 4$. Selected bond lengths are given in Table 1. Six nitrogen atoms of Hpy-DAPP ligand constitute the first coordination sphere around the Fe^{II} atom (Figure 2). The ligand, upon coordination to iron(II), forms three five-membered and two six-membered chelate cycles. It should be noted that three pyridine rings (or three aliphatic amino groups) of the Hpy-DAPP ligand can have either a facial or a meridional arrangement, which gives rise, in principle, to a number of isomers. An octahedral coordination leads to the possible existence of two stereoisomers (Δ or Λ configuration). In [Fe(Hpy-DAPP)]$(BF_4)_2$, the ligand adopts a *fac* configuration and the unit cell contains two pairs of symmetry-related left-handed and right-handed enantiomers.

Table 1. Selected bond lengths [Å] for [Fe(Hpy-DAPP)]$(BF_4)_2$.[a]

	T = 298 K	T = 130 K	T = 90 K
Fe(1)–N(1)	2.208(3)		2.009(5)
Fe(1)–N(1A)		2.140(3)	
Fe(1)–N(1B)		2.034(10)	
Fe(1)–N(2)	2.238(2)	2.152(4)	2.128(4)
Fe(1)–N(3)			2.085(6)
Fe(1)–N(3A)	2.151(4)	2.084(8)	
Fe(1)–N(3B)	2.217(5)	2.104(10)	
Fe(1)–N(4)	2.181(2)	2.071(4)	2.049(4)
Fe(1)–N(5)	2.191(2)	2.030(5)	2.033(5)
Fe(1)–N(6)	2.235(2)	2.079(5)	2.061(4)

[a] Estimated standard deviations in the least significant digits are given in parentheses.

High-Spin Complex Structure (T = 298 K)

The $[FeN_6]$ coordination core is severely distorted at room temperature, and the Fe–N distances fall within the range 2.151(4)–2.238(2) Å (see Table 1). The average Fe–N distance is equal to 2.206 Å, typical for iron(II) in the HS state. The octahedron is axially elongated along the N2–Fe–N6 direction, which can be seen as a pseudo-Jahn–Teller distortion. The secondary N3 amino aliphatic atom is disordered over two positions (Figure 3, a), with an occupancy close to 0.5:0.5. The two Fe–N3(A) and Fe–N3(B) distances are rather different and equal to 2.151(4) and 2.217(5) Å, respectively. The N–Fe–N angles between the adjacent and the opposite nitrogen atoms fall within the range 73.7(2)–111.6(2)° and 160.5(2)–166.5(1)°, respectively. The largest deviation (74–78°) from 90° is observed in three five-membered chelate cycles due to steric strain. In contrast, the N–Fe–N angles in the FeN2C7C8C9N1 and FeN2C16C17C18N3(A/B) six-membered chelate cycles are close to the ideal octahedral value, probably owing to the flexibility of the amino aliphatic chain. The former metallocycle adopts a *chair* conformation (Figure 3, a).

The BF_4 counterions were found to be badly disordered at room temperature (Figure 2). This disorder was modeled over two orientations in a 0.5:0.5 occupation ratio. The disordered groups are represented as a superposition of two tetrahedra with a unique position for the B atoms and eight different orientations for the F atoms. However, the large values of the anisotropic displacement parameter for the F atoms indicate that the disorder model with only two positions for the BF_4 groups, derived from the SHELXS-97 program, is not fully satisfactory. It is therefore very likely that both counterions are disordered over several rather close orientations at room temperature.

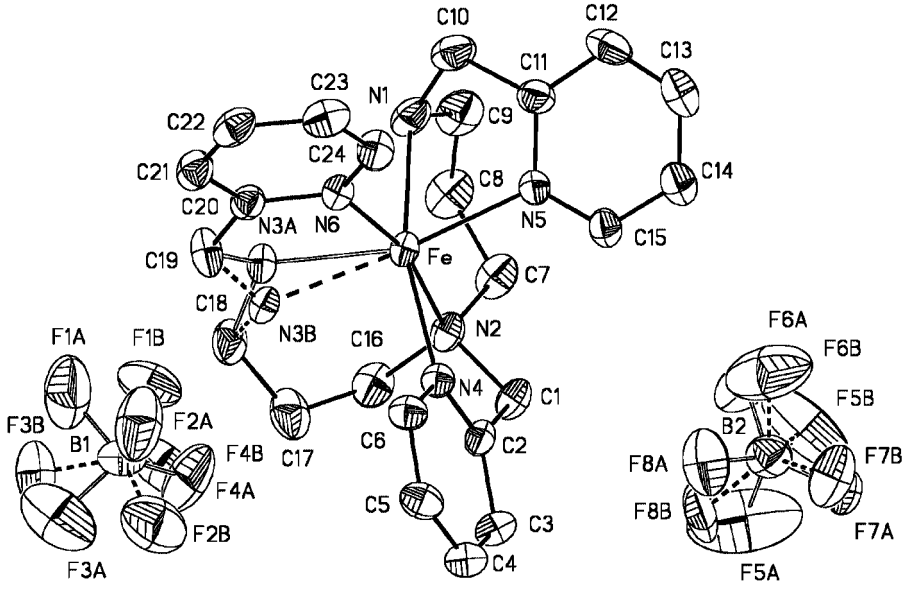

Figure 2. ORTEP view of [Fe(Hpy-DAPP)]$(BF_4)_2$ at 298 K. Ellipsoids enclose 30% probability. The hydrogen atoms have been omitted for clarity.

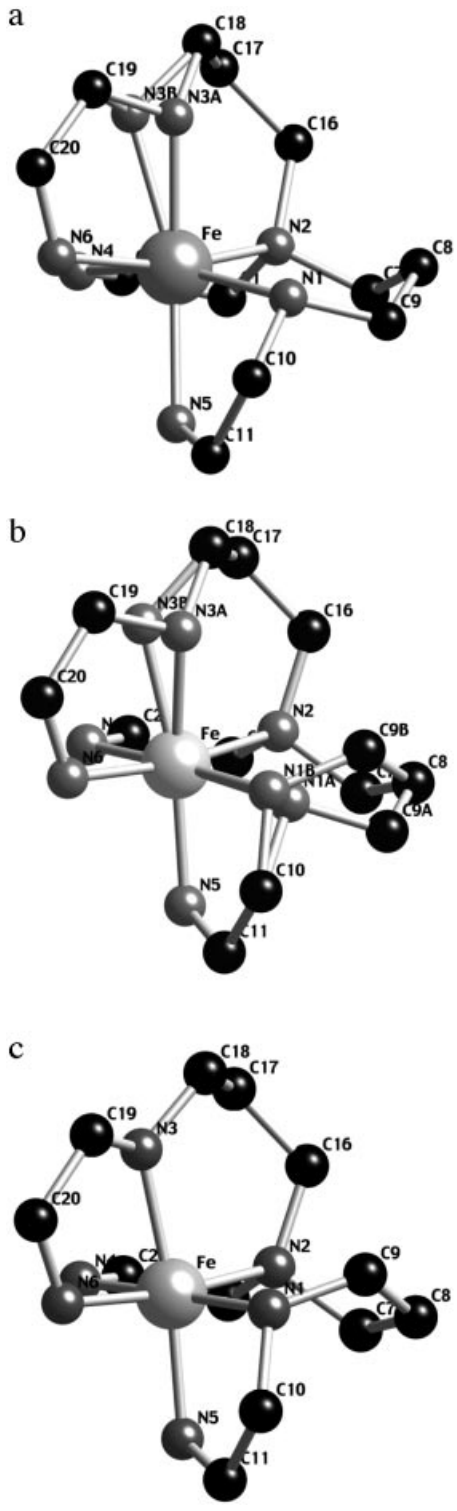

Figure 3. Fragment of the molecular structure of [Fe(Hpy-DAPP)]$(BF_4)_2$ at 298 K (a), 130 K (b), and 90 K (c).

Figure 4 displays a projection of the crystal structure on the *ac* plane. The cohesion between the cation complexes is achieved by numerous indirect hydrogen bonds passing via the fluorine atoms of both counteranions (Table 2). The fluorine atoms of the B1 tetrafluoroborate ion are strongly involved in the formation of sixteen H-bonds, namely four intramolecular bonds with the N1 atom, two intra- and two intermolecular bonds with the disordered N3 atom, and three intra- and five intermolecular bonds with C13 and C19 atoms, respectively. The intermolecular interactions concerning the B1 counterion link the molecules related by the symmetry operation x, $0.5 - y$, $0.5 + z$ into infinite chains that propagate in the *c* direction. The fluorine atoms of the B2 tetrafluoroborate anions, much less involved in the hydrogen bonding, take part in only a few H-bonds (Table 2). They link the molecules from neighboring infinite chains into a three-dimensional network. The H-bonds with the B2 counterions spread in the directions corresponding to the two diagonals in the *ab* plane.

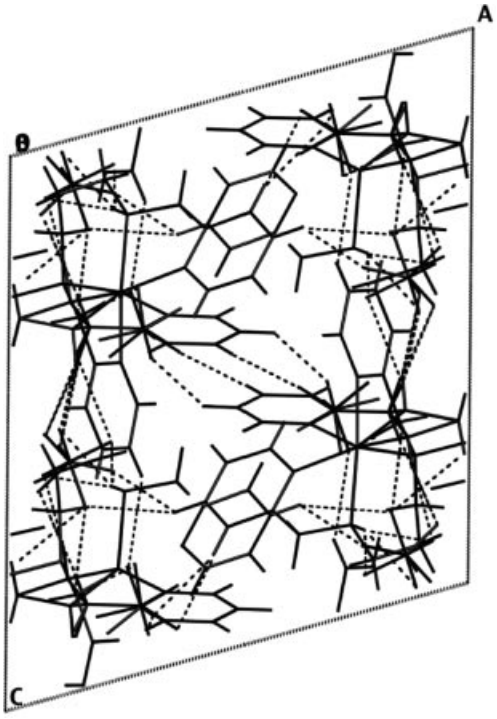

Figure 4. Projection of the molecular structure on the *ac* plane showing the H-bonding network at 298 K.

T = 130 K (Cooling Mode)

The main feature of the structure is the disorder enhancement within the Fe^{II} coordination core despite the lowering of the temperature. The disorder of the N3 amino aliphatic group over two equally occupied sites is retained (Figure 3, b). Moreover, the second amino aliphatic N1 atom, as well as the adjacent C9 methylene group, which are only slightly agitated at room temperature, were resolved to be also disordered over two A and B sites with a 0.5:0.5 occupancy ratio. At 130 K, the FeN2C7C8C9(A)N1(A) and FeN2C7C8C9(B)N1(B) six-membered chelate cycles adopt two different conformations. The former, as at room temperature, has a *chair* conformation, whereas the latter adopts a *twist-boat* conformation (Figure 3, b). At this temperature, the geometry of the $[FeN_6]$ octahedron reflects the changes conforming to a partial HS→LS transition. The distances in the coordination core decrease (Table 1) and the average Fe–N distance decreases to 2.087 Å.

Table 2. Interatomic distances [Å] and angles [°] for the hydrogen-bonding interactions in[Fe(Hpy-DAPP)]$(BF_4)_2$.[a,b]

D–H···A	D–H	H···A	D···A	D–H···A
298 K				
N(1)–H(1N)···F(1A)[1]	0.910	2.547	3.336(7)	145.4
N(1)–H(1N)···F(1B)[1]	0.910	2.430	3.242(7)	148.7
N(1)–H(1N)···F(2A)[1]	0.910	2.097	2.944(6)	154.4
N(1)–H(1N)···F(3B)[1]	0.910	2.343	3.170(6)	151.0
N(3A)–H(3NA)···F(3A)[1]	0.910	2.135	3.007(9)	160.2
N(3A)–H(3NA)···F(3B)[1]	0.910	2.229	3.134(9)	172.6
N(3B)–H(3NB)···F(4A)[2]	0.910	2.498	3.301(9)	147.3
N(3B)–H(3NB)···F(4B)[2]	0.910	2.408	3.118(9)	134.9
C(12)–H(12A)···F(7A)[1]	0.930	2.483	3.378(9)	161.6
C(13)–H(13A)···F(2A)[3]	0.930	2.543	3.240(6)	132.0
C(19)–H(19A)···F(1A)[2]	0.970	2.418	3.243(9)	142.7
C(19)–H(19A)···F(1B)[2]	0.970	2.538	3.299(7)	135.4
C(19)–H(19A)···F(4B)[2]	0.970	2.322	3.280(8)	169.2
C(19)–H(19B)···F(2B)[1]	0.970	2.483	3.139(8)	124.8
C(19)–H(19C)···F(1A)[2]	0.970	2.297	3.243(9)	164.9
C(19)–H(19D)···F(3A)[1]	0.970	2.535	3.443(8)	155.7
C(19)–H(19D)···F(2B)[1]	0.970	2.240	3.139(8)	153.8
C(21)–H(21A)···F(7A)[4]	0.930	2.487	3.212(5)	135.0
C(22)–H(22A)···F(7B)[2]	0.930	2.517	3.396(5)	157.7
130 K				
N(1A)–H(1NA)···F(1)[1]	0.930	2.450	3.22(3)	140.7
N(1B)–H(1NB)···F(1)[1]	0.930	2.332	3.04(2)	132.6
N(1A)–H(1NA)···F(3)[1]	0.930	2.493	3.39(3)	163.3
N(1B)–H(1NB)···F(3)[1]	0.930	2.542	3.21(1)	129.6
N(3A)–H(3NA)···F(3)[1]	0.930	2.134	3.03(1)	162.5
N(3B)–H(3NB)···F(4)[2]	0.930	2.394	3.17(1)	141.2
C(9A)–H(9A)···F(5)[5]	0.990	2.210	2.82(2)	118.6
C(9B)–H(9C)···F(3)[1]	0.990	2.456	3.00(1)	113.9
C(12)–H(12A)···F(7)[1]	0.950	2.455	3.39(1)	169.4
C(13)–H(13A)···F(2)[3]	0.950	2.483	3.32(1)	146.3
C(19)–H(19A)···F(4)[2]	0.990	2.328	3.30(1)	166.7
C(19)–H(19B)···F(2)[1]	0.990	2.531	3.19(1)	123.9
C(19)–H(19D)···F(2) [1]	0.990	2.222	3.19(1)	162.8
C(24)–H(24A)···N(5)[1]	0.950	2.600	3.130(7)	115.6
90 K				
N(1)–H(1N)···F(1)[1]	0.930	2.403	3.087(8)	130.3
N(1)–H(1N)···F(3)[1]	0.930	2.497	3.209(9)	133.5
N(3)–H(3N)···F(4)[2]	0.930	2.381	3.186(1)	144.7
C(7)–H(7A)···N(5)[1]	0.990	2.616	3.167(8)	115.2
C(9)–H(9B)···F(3)[1]	0.990	2.562	3.05(1)	110.6
C(12)–H(12A)···F(7)[1]	0.950	2.455	3.39(1)	166.3
C(13)–H(13A)···F(2)[3]	0.950	2.548	3.35(1)	142.3
C(16)–H(16A)···F(5)[6]	0.990	2.539	3.27(1)	130.7
C(19)–H(19B)···F(2)[1]	0.990	2.316	3.18(1)	145.7
C(24)–H(24A)···N(5)[1]	0.950	2.613	3.133(7)	114.9

[a] Symmetry operations: (1) x, y, z; (2) x, $0.5 - y$, $0.5 + z$; (3) $1 - x$, $0.5 + y$, $0.5 - z$; (4) $1 - x$, $-0.5 + y$, $0.5 - z$; (5) $1 - x$, $1 - y$, $-z$; (6) $-1 + x$, y, z. [b] Estimated standard deviations in the least significant digits are given in parentheses.

Several models of splitting of the BF_4 anions at 130 K were tested. However, the best result was obtained for an ordered model. This suggests that the tetrafluoroborate anions undergo an order–disorder transition above 130 K. The anisotropic thermal parameters for the fluorine atoms are considerably reduced relative to 298 K. Nevertheless, they remain slightly higher than those for the other atoms.

Upon lowering the temperature to 130 K, the shortening of the unit-cell parameters and the bond lengths due to both thermal contraction and partial spin-transition occurs. Relative to 298 K, the unit-cell volume decreases by 5.3% (151 Å^3), although the crystal packing is similar to that at room temperature. The number of H-bonds is lower but the topology of their propagation in the crystal is quite similar (Table 2). As above, the B1 tetrafluoroborate anions participate in the formation of intra- and intermolecular interactions that result in infinite chains of H-bound complex cations spreading in the *c* direction. The intermolecular distances connected with H-bonding (Table 2) are slightly reduced, showing a relative strengthening of the intermolecular interactions upon cooling.

Low-Spin Complex Structure (T = 90 K)

At this temperature, according to the magnetic and Mössbauer data (vide infra), the LS sample contains small amounts of the HS isomer (10%). Despite the presence of a residual HS fraction, the structural characteristics found at 90 K are close to those usually observed for LS complexes.

The main result of the structural determination at this temperature is the disappearance of disorder in the positions of both N1 and N3 secondary amino aliphatic nitrogen atoms observed at 130 K (Figure 3, c). Despite a general decrease, the anisotropic displacement parameter values for several atoms (N1, N3, and C9, as well as F2, F3, F5, and F6) remain slightly higher than those for the other atoms. This can be explained by the contribution of disorder introduced by the residual HS fraction. The FeN2C7C8C9N1 six-membered chelate cycle adopts a *twist-boat* conformation (Figure 3, c), whereas the FeN2C16C17C18N3 metallacycle has an intermediate conformation between the *chair* and *half-boat* ones.

Upon cooling, the metal–ligand distances in the $[FeN_6]$ coordination core become shorter (Table 1), in full accordance with the HS→LS transition. The reductions of the Fe–N distances are 0.199 (Fe–N1), 0.110 (Fe–N2), 0.099 (Fe–N3), 0.132 (Fe–N4), 0.158 (Fe–N5), and 0.174 Å (Fe–N6), relative to the room-temperature values. The N–Fe–N angles also vary in the direction of a more regular geometry of the $[FeN_6]$ octahedron.

At 90 K, the unit-cell volume decreases by 5.94% (168 Å^3) relative to that at 298 K due to both the lattice thermal contraction and the shortening of the Fe–N distances upon spin transition. The anisotropy of the unit-cell contraction amounts to 3.23, 1.01, and 1.48% for the *a*, *b*, and *c* axes, respectively, and 0.57% for the β angle. The network of intermolecular contacts represented by hydrogen bonds is rather similar to that for the HS form (Table 2): the crystal packing consists of chains of molecules spreading in the *c* direction. The cohesion within the chains is provided by H-bonding through the B1 tetrafluoroborate anion, whereas between the chains it mainly occurs via the B2 counterion.

Mössbauer Data

Mössbauer spectra for [Fe(Hpy-DAPP)]$(BF_4)_2$ were recorded on two different batches of freshly prepared sam-

ples. Within the experimental error, the Mössbauer parameters were found to be the same for the two syntheses. Figure 5 shows some representative spectra at different temperatures. The values of the main Mössbauer parameters obtained from a least-square fitting procedure are listed in Table 3 for the whole temperature range. The room-temperature Mössbauer spectrum consists of a unique quadrupole-split doublet with parameters typical for iron(II) in the HS state (δ = 0.955 mm s^{-1}, ΔE_q = 1.848 mm s^{-1}). The Mössbauer spectra at lower temperatures can be best fitted with two doublets corresponding to HS and LS iron(II) species. The Mössbauer area fraction [$A_{HS}/(A_{HS} + A_{LS})$] is plotted as a function of temperature (in the cooling mode) in Figure 6. It reveals the same two-step spin-crossover behavior as the magnetic measurements. The low-temperature residual HS fraction was found to be significantly different in the two series of Mössbauer measurements. We attribute this difference to the somewhat different cooling procedure in the two cases. To check this hypothesis, we carried out a series of thermal quenching experiments down to 80 K at different cooling rates (0.1, 1, 10, and 50 K min^{-1}). The HS fractions obtained at different cooling rates are included in Figure 6. At the lowest cooling rate we obtained about 8% HS residue, while at 10 and 50 K min^{-1} the trapped HS fraction reached 31 and 32%, respectively.

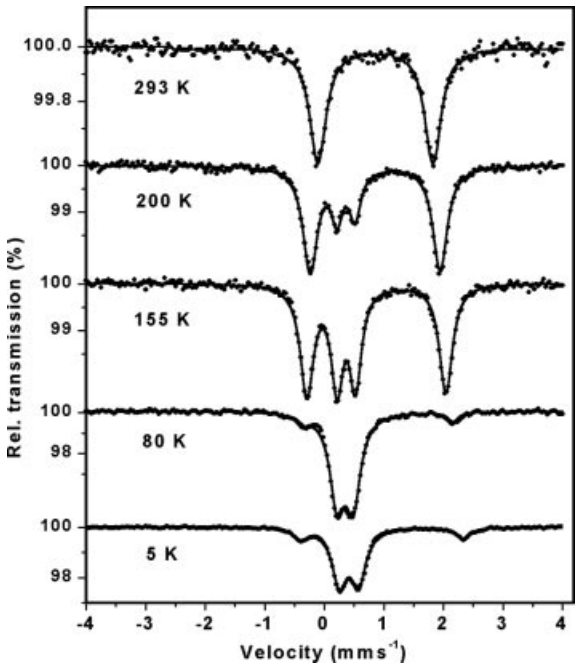

Figure 5. Representative Mössbauer spectra of [Fe(Hpy-DAPP)](BF$_4$)$_2$. The solid lines represent fitted curves.

The thermal variation of the Mössbauer parameters in the vicinity of the inflexion point (80–200 K) was carefully analyzed. Figures showing the evolution of the isomer shift (δ), half-height width (Γ), quadrupole splitting (ΔE_q) of the HS and LS Mössbauer lines, and the logarithm of the total Mössbauer spectrum area as a function of the temperature in the cooling cycle are provided as Supporting Information. Due to the second-order Doppler effect, both the HS and LS isomer shifts increase almost linearly with decreasing temperature. One can observe a slight deviation from the linear behavior around 125 K, but it hardly exceeds the experimental incertitude. The line widths of the HS and LS Mössbauer lines show an opposing tendency: while the former decreases, the latter increases slightly with decreasing temperatures. The thermal variation of Γ_{LS} displays a jump between 125 and 117.5 K. For Γ_{HS} the statistical errors become too high around these temperatures due to the small proportion of HS molecules. As a general ten-

Table 3. Least-squares fitted Mössbauer data for [Fe(Hpy-DAPP)](BF$_4$)$_2$.[a]

	HS			LS			$A_{HS}/(A_{tot})$
T [K]	δ [mm s^{-1}]	ΔE_q [mm s^{-1}]	$\Gamma/2$ [mm s^{-1}]	δ [mm s^{-1}]	ΔE_q [mm s^{-1}]	$\Gamma/2$ [mm s^{-1}]	
293*	0.955(2)	1.848(4)	0.159(3)	–	–	–	1
250	0.997(2)	2.103(3)	0.155(3)	0.49(1)	0.29(2)	0.10(1)	0.91(1)
200*	1.011(3)	2.221(5)	0.149(4)	0.50(1)	0.30(1)	0.13(1)	0.76(1)
200	1.017(1)	2.265(3)	0.150(2)	0.508(3)	0.317(5)	0.119(4)	0.733(5)
185	1.026(2)	2.317(3)	0.147(2)	0.507(3)	0.319(4)	0.118(3)	0.680(5)
170	1.032(2)	2.371(3)	0.143(2)	0.516(2)	0.319(3)	0.121(3)	0.615(5)
155	1.039(1)	2.425(3)	0.137(2)	0.514(2)	0.321(3)	0.122(2)	0.555(4)
150*	1.033(2)	2.431(4)	0.143(3)	0.524(2)	0.326(3)	0.124(3)	0.508(2)
140	1.046(2)	2.465(4)	0.138(3)	0.517(2)	0.317(3)	0.125(3)	0.519(5)
132.5	1.053(2)	2.494(4)	0.139(3)	0.514(2)	0.315(3)	0.126(2)	0.496(5)
125	1.054(2)	2.512(4)	0.139(3)	0.523(2)	0.320(3)	0.129(2)	0.467(6)
117.5	1.070(3)	2.521(5)	0.133(4)	0.504(2)	0.303(4)	0.146(3)	0.389(7)
110	1.058(3)	2.562(6)	0.142(5)	0.516(1)	0.300(2)	0.144(2)	0.294(6)
100*	1.053(4)	2.594(8)	0.122(7)	0.528(1)	0.300(2)	0.139(2)	0.19(1)
95	1.043(6)	2.62(1)	0.13(1)	0.523(1)	0.296(2)	0.145(2)	0.14(1)
80	1.06(1)	2.62(2)	0.11(1)	0.50(1)	0.277(2)	0.150(2)	0.08(1)
5*	1.128(4)	2.806(8)	0.137(6)	0.557(1)	0.326(2)	0.150(1)	0.16(1)

[a] δ: isomer shift (with reference to metallic iron at 293 K); ΔE_q: quadrupole splitting; Γ: half-height width; A_{HS}: area of HS doublet; A_{tot}: total Mössbauer spectrum area. The error bars of statistical origin are given in parentheses. Temperature values marked with (*) correspond to measurements on a separate batch of synthesis.

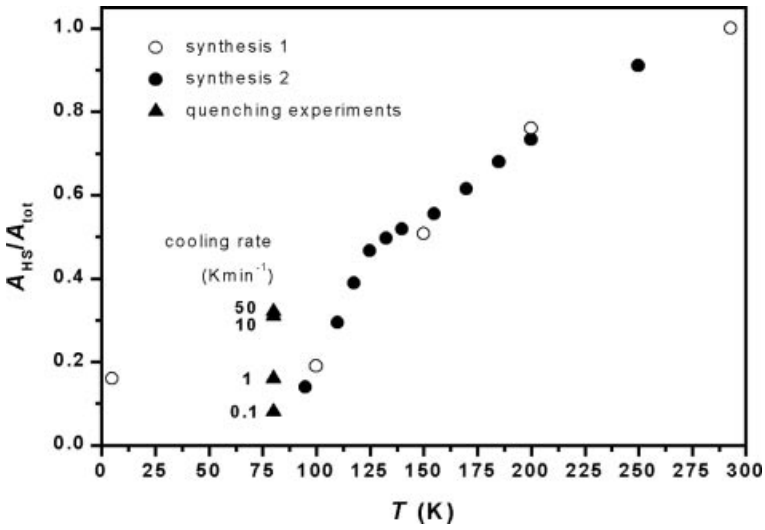

Figure 6. Temperature dependence of the Mössbauer area ratio for [Fe(Hpy-DAPP)](BF$_4$)$_2$ (two batches of synthesis). See the text for explanation of the quenching experiments.

dency, however, the HS quadrupole splitting increases between 200 and 80 K while it remains almost constant in the LS state. This behavior of ΔE_q is typical for iron(II) ions in the HS and LS spin states.[7] A closer inspection of quadrupole splittings reveals a jump in the ΔE_q^{LS} values between 125 and 117.5 K and a less monotonous increase of ΔE_q^{HS} below 132 K. This latter observation may, however, be hampered by increasing experimental errors when the HS fraction decreases. The natural logarithm of the Mössbauer line area as a function of temperature shows the continuous increasing tendency with decreasing temperature without any noticeable discontinuity.

Electronic Structure Calculations

The molecular geometry of the isolated [Fe(Hpy-DAPP)]$^{2+}$ complex cation was firstly optimized in the HS and LS states. The optimized bond lengths in the LS and HS states reproduce the geometry found from the X-ray study at 90 K and 300 K, respectively, quite reasonably. All attempts to find another equilibrium geometry of the complex by modifying the departure geometry in the optimization procedure were unsuccessful. This means that the disorder in the spin transition complex is not due to the existence of several intrinsic complex conformations that are close in energy. At the next step, the single-point calculations were performed for the molecular structures obtained by X-ray crystallography at different temperatures. The calculations with the structure observed at 90 K correctly reproduce the ground LS state, with an energy gap to the HS state of 33 kJ mol^{-1}. If the molecular structures manifest a disorder, as is found at 300 and 130 K, the calculations were done for each observed geometry. Thus, with the 300-K structure the energies of the HS and LS states were calculated separately for the geometries with N3(A) and N3(B). In both cases, the HS state lies lower than the LS state of the same geometry. The energy gap is equal to 115 and 121 kJ mol^{-1} for the N3(A) and N3(B) positions, respectively. These two values are quite similar, which suggests that the geometry with the N3(A) position is slightly closer to the spin transition. Disorder was observed for the two nitrogen atoms, as at 130 K, and as, a priori, we have no grounds to presume a correlation between the N1 and N3 positions, four geometries were considered, corresponding to the combinations N1(A)N3(A), N1(A)N3(B), N1(B)N3(A), and N1(B)N3(B). The ground HS state was obtained for the first two geometries with the energy gaps to the excited LS state equal to 23 and 14 kJ mol^{-1} for N1(A)N3(A) and N1(A)N3(B), respectively. An inverse order of the spin levels was found for the N1(B)N3(A) and N1(B)N3(B) geometries, with the LS state stabilized by 6 and 17 kJ mol^{-1}, respectively.

The preference of the N1(B)N3(B) geometry for the formation of the LS state directly follows from comparison of Mulliken atomic charges, which are equal to –0.54 and –0.55 for N1(B) and N3(B), respectively, and to –0.48 for N1(A) and N3(A). These numbers indicate that the N1(B) N3(B) geometry corresponds to a stronger crystal field. This effect is also displayed in the energies of the molecular orbitals. All antibonding orbitals of the d block have about the same energies for N1(A)N3(A) and N1(B)N3(B), besides that originating from $d_{x^2-y^2}$, which is stabilized in N1(A)N3(A) by 55 kJ mol^{-1}. The antibonding character of the MO in the N1(A)N3(A) conformation is counterbalanced by a bonding behavior between the 2p atomic orbital of N1 and the $d_{x^2-y^2}$ atomic orbital of the Fe atom (Figure 7).

The results of calculations unambiguously show that the structural disorder revealed at 130 K by X-ray crystallography is accompanied by the coexistence in the crystal of complexes in the HS and LS states. Two statistically possible geometries result in the HS ground state, whereas for two others the order of spin states is the same as at low temperature.

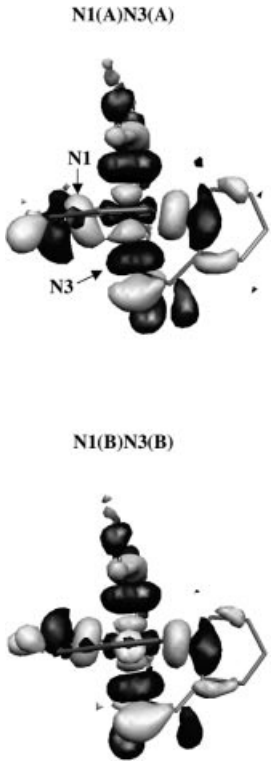

Figure 7. Three-dimensional plot of the $d_{x^2-y^2}$-containing molecular orbital in the $[Fe(Hpy\text{-}DAPP)]^{2+}$ complex cation.

Discussion

The magnetic measurements of the [Fe(Hpy-DAPP)]$(BF_4)_2$ complex display a two-step spin transition. Such spin transitions have been reported for both binuclear[8] and mononuclear[9,10] Fe^{II} spin-crossover compounds. Until now, the origin of two steps within the family of mononuclear compounds has been associated with the presence of two crystallographically inequivalent iron(II) sites in the unit cell. If two metal sites coexist whatever the temperature,[9] the thermal two-step spin transition can occur without change of the crystallographic symmetry group. The structural distinction between the two lattice sites leads to different transition temperatures. Two inequivalent Fe^{II} sites can also appear upon cooling as a result of a crystallographic phase transition accompanied by a change of the space group.[10] It is interesting to note that the extensively studied mononuclear complex $[Fe(2\text{-pic})_3]Cl_2\cdot EtOH$[11] has been considered during the last 25 years as the only example of an iron(II) compound with a unique metal site[12] for which a two-step spin transition[13] takes place without any crystallographic phase transition. This phenomenon was interpreted in terms of coexisting positive and negative interactions,[8a] respectively, over a long and short range.[14a–14c] However, a recent detailed X-ray reinvestigation of $[Fe(2\text{-pic})_3]Cl_2\cdot EtOH$[10b] has shown that the expected negative correlations exhibit a long-range character in the plateau temperature range. Two steps on the thermal spin-transition curve result from two successive re-entrant structural phase-transitions of the order–disorder type. Nevertheless, the existence of HS-LS pairs with short correlation lengths was found for the photoinduced state.[14d]

The striking feature of the two-step spin-transition compound [Fe(Hpy-DAPP)]$(BF_4)_2$ consists in the absence of two crystallographically inequivalent iron(II) lattice sites, as well as a crystallographic phase transition accompanied by a change of space group. The most important peculiarity of the HS structure of the [Fe(Hpy-DAPP)]$(BF_4)_2$ complex is the disorder of the secondary N3 amino aliphatic atom over two positions (Figures 2 and 3a). A possible origin of the disorder of the N3 atoms, which constitute the first coordination sphere in iron(II), may be looked for in their strong involvement in H-bonding with their own and neighboring B1 counterions (Figure 8). Each B1 counterion is simultaneously attached by hydrogen bonds to the N3 atom belonging to its own complex cation and to the N3 atom of the neighboring complex (symmetry operation x, $0.5 - y$, $0.5 + z$), thus forming infinite chains of complexes in the c direction. One can suppose that the strong H-bonding of the same N3 atom with two different counterions might produce appreciable constraint in the position of the N3 atom, thereby favoring a disorder between the A and B positions. This disorder is facilitated by a high flexibility of the N3-containing six-membered chelate cycle. At room temperature, the N1 amino aliphatic atom is also strongly involved in hydrogen bonding but only with its own B1 counterion. At room temperature, in contrast to the N3 atom, the position of the N1 atom is ordered.

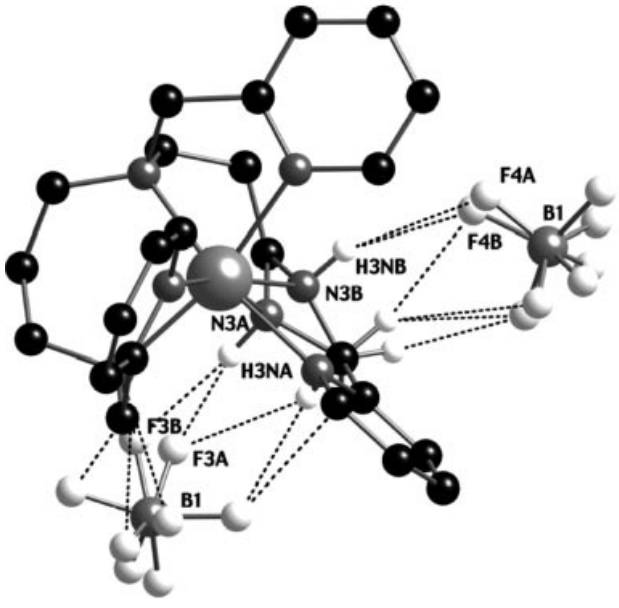

Figure 8. View of the hydrogen bonds of the N3 atom with its own and neighboring (symmetry operation: x, $0.5 - y$, $0.5 + z$) B1 counterions at 298 K. The labels for the other atoms have been omitted for clarity.

The structure determination at 130 K, corresponding to the inflexion point on the magnetic curve when the conversion from high to low spin reaches 50%, shows some new features. The disorder of the N3 amino aliphatic atom observed at room temperature is attended by the distribution

of the N1 atom between the two A and B positions. Moreover, the C9 methylene atom directly linked to the N1 atom is also equally distributed over C9(A) and C9(B) sites, which are stabilized by two new hydrogen bonds with the B1 and B2 counterions (Table 2). The two N1(A) and N1(B) positions are very close, whereas the C9(A) and C9(B) positions are rather distant one from another. The presence of the two sites for atoms N1 and C9 causes the two conformations of the N2C7C8C9N1Fe six-membered metallacycle (Figure 3, b). The N2C7C8C9(A)N1(A)Fe cycle has a *chair* conformation that is very close to that observed at room temperature (Figure 3, a), whereas the *twist-boat* conformation N2C7C8C9(B)N1(B)Fe appears in the course of spin conversion. This result strongly suggests that the spin conversion above the inflexion point is accompanied by the conformational change in the ligand. The crystallographic data obtained at 170 K confirm the coexistence of the C9(A) and C9(B) sites already at this temperature. However, the conformational motion in the complex is not drastic enough to modify the space group. It is important to underline that the 1:1 ratio of the HS and LS forms at 130 K coincides with the distribution of the N2C7C8C9N1Fe chelate cycle over two conformations.

Upon lowering the temperature to 90 K, the average metal–ligand distance becomes 0.142 Å shorter than at room temperature, which conforms to the occurrence of the HS→LS transition. The disorder found at 130 K for the positions of the N1, N3, and C9 atoms disappears at 90 K. The N2C7C8C9N1Fe metallacycle adopts a unique *twist-boat* conformation at 90 K (Figure 3, c). It should be noted that the geometry of the N2N7N8N9N1Fe chelate cycle in the LS complex is very close to that observed for the N2C7C8C9(B)N1(B)Fe metallacycle at 130 K (Figure 3, b). One may therefore conclude that the HS→LS transition in the complex is accompanied by order–disorder phenomena in conjugation with a conformational change in the ligand.

Let us now consider the relationship between the disorder in the [FeN$_6$] coordination core and the magnetic behavior of the system. A priori, the mononuclear [Fe(Hpy-DAPP)](BF$_4$)$_2$ complex without any crystallographic phase transition should be expected to display a one-step spin transition. Nevertheless, the magnetic measurements show the two steps in the spin transition. The presented X-ray data for [Fe(Hpy-DAPP)](BF$_4$)$_2$ do not contradict the basic assumption of two-step transition models, which involves the competition between positive and negative interactions[8a] possibly giving rise to short-range negative correlations[14a–14c] or to LS-HS sub-lattice ordering.[8a] However, our crystallographic data suggest that the origin of the two-step transition in [Fe(Hpy-DAPP)](BF$_4$)$_2$ can also be looked for in the [FeN$_6$] coordination core ordering. At room temperature, the distribution of the N3 amino aliphatic atom over two lattice positions preforms two geometries of the coordination core around the crystallographically unique Fe^{II} center, with N3(A) and N3(B), respectively (Figure 3, a). Both geometries correspond to the HS state at 298 K. The systematic variation of the Mössbauer line widths for the HS doublet above 160 K (see Supporting Information) might suggest the existence of two different iron(II) environments with very similar Mössbauer parameters. However, these changes are very small and no reliable fit could be obtained with two doublets in the whole high temperature range. The congruency of two doublets corresponding to two different coordination geometries due to the high temperature disorder of counterions, as has been proposed for the compound [Fe(mtz)$_6$](BF$_4$)$_2$,[15] cannot, however, be excluded. Upon lowering the temperature from 298 to 230 K, the $\chi_M T$ value changes slightly, thus showing that the complex remains predominantly in the HS state. A further decrease of temperature leads to a continuous reduction of the $\chi_M T$ value, which indicates the beginning of spin transition. On cooling, both tetrafluoroborate counteranions become less agitated. The reduction of the counteranions' motion leads to their more regular arrangement in the crystal lattice, resulting in some modifications of the H-bonds between the B1 counteranions and the secondary amino aliphatic atoms. These modifications induce subtle perturbations of the N1 and N3 nitrogen atoms directly coordinated to the iron(II) center and affect the ligand field strength, initiating, in turn, the spin transition. The inflexion point on the magnetic curve denotes that at 130 K the spin transition is complete in half the sites whereas the other half remain in the HS state. At this temperature four possible coordination cores can be formally distinguished around the same Fe^{II} atom. These four coordination cores may include, in addition to the N2N4N5N6 atoms, the pairs N1(A)N3(A), N1(A)N3(B), N1(B)N3(A), or N1(B)N3(B). The 0.5:0.5 occupation ratio for both the N1 and N3 atoms suggests that either all four combinations, or only two of them, namely N1(A)N3(A) and N1(B)N3(B), exist. The difference in the average Fe–N distances in the four cores (2.093, 2.096, 2.075, and 2.078 Å) is not significant enough to allow a proper identification of the HS and LS sites.

It has been demonstrated previously that not only metal–ligand distances but also angular distortions can modulate the ground-state spin.[16] As has been noted above, the geometries of the N2C7C8C9(B)N1(B)Fe chelate cycle at 130 K and the N2C7C8C9N1Fe chelate cycle in the LS complex at 90 K are very similar, with both being in the *twist-boat* conformation (see parts b and c in Figure 3). One may suppose that the LS coordination core at 130 K should involve the N1(B) atom. At 130 K, two coordination site geometries, from four formally possible, contain the N1(B) atom. The quantum-chemical calculations show that both the N1(B)N3(A) and N1(B)N3(B) pairs lead to the LS state. However, a very short distance (2.669 Å) between the N1(B) and N3(A) atoms, as well as between the attached hydrogen atoms (1.846 Å), should lead to an important steric strain (note that the van der Waals radii for the nitrogen and hydrogen atoms are 1.55 and 1.20 Å, respectively). Moreover, the presence of H-bonds between the N1(B) and N3(A) atoms must also be rejected due to the rather small N–H···N angles of 95.7° and 104.0°. Thus, it may be concluded that the LS site at 130 K contains the N1(B) and N3(B) atoms, i.e. the N1(B)N3(B) and N1(A)N3(A) pairs conform

to the LS and HS isomers, respectively. The spin conversion in the N1(B)N2N3(B)N4N5N6 core is accompanied by a conformational transition in the ligand, whereas the high-spin N1(A)N2N3(A)N4N5N6 core retains a geometry close to that observed at room temperature.

The first step in the spin transition is very gradual but the second one is abrupt, with a hysteresis loop of 4 K. The change in the abruptness in the spin transition may be explained by the strengthening of intermolecular interactions, which leads to a higher cooperativity in the low-temperature step. The second step in the spin conversion is also associated with a conformational change in the ligand similar to that observed for the first step. So, two geometries of the $[FeN_6]$ coordination core, generated by order–disorder phenomena at room temperature, in the course of the spin transition converge to a unique geometry of the Fe^{II} coordination site. The hysteresis in the low-temperature step is not connected either with a crystallographic phase transition or with strong changes of the unit-cell parameters and/or topology of the cooperative interactions.[6] One can suppose that the hysteresis results from a slow conformational transition in the ligand at low temperature. Indeed, the efficient quenching of the HS form indicates that the HS → LS relaxation is very slow at around 80 K. In order to throw more light on this phenomenon, further experiments will be necessary (magnetic measurements at different scan rates, thermal quenching and photoswitching experiments followed by relaxation studies).

In summary, we would like to underline that our studies suggest that $[Fe(Hpy\text{-}DAPP)](BF_4)_2$ is the first example of a spin-transition system that displays a disorder in the first coordination sphere of the metal center. Two different geometries of the $[FeN_6]$ coordination core generated by the disorder in the ligand may be at the origin of the two-step spin-transition behavior of the system. However, keeping in mind that it took 25 years to clarify the origin of the two-step transition in $[Fe(2\text{-}pic)_3]Cl_2{\cdot}EtOH$,[10b,12–14] we consider that further advanced crystallographic studies are needed to verify this hypothesis. The HS → LS transition is conjugated with the conformational change in the chelate cycle, and other examples of conformationally driven electronic transitions are known in the literature.[17] Conformational transformations in the solid state have been observed for thermochromic systems and electron-transfer mixed-valence complexes. However, this phenomenon for spin-transition systems in the solid state has not been described until now.

Experimental Section

Chemistry: All reagents and solvents used in this study are commercially available and were used without further purification. All syntheses involving Fe^{II} species were carried out in deoxygenated solvents under an inert atmosphere of N_2 using glovebox techniques. [Bis(3-aminopropyl)(2-pyridylmethyl)amine] (DAPP) was obtained according to the procedure we have recently reported.[6] $FeCl_2{\cdot}2H_2O$ was prepared as described elsewhere.[18] ^1H NMR spectra were recorded in $CDCl_3$ on a Bruker AC200 spectrometer operating at 200 MHz.

Ligand Synthesis (Hpy-DAPP): A mixture of DAPP (96 μL, 0.5 mmol) and 2-pyridinecarboxaldehyde (107 mg, 1 mmol) in methanol (15 mL) was refluxed under argon for 15 min. Then, an excess of $NaBH_4$ (100 mg) was added in several small portions. The solution was allowed to stand overnight at room temperature and the solvent was evaporated under vacuum. After successive extraction of the crude product with $CHCl_3$ and Et_2O, 180 mg of pure HpyDAPP was obtained as a pale-yellow oil. ^1H NMR ($CDCl_3$): δ = 8.53–7.08 (m, 12 H, aromatic H's), 3.84 (s, 4 H, CH_2), 3.68 (s, 2 H, CH_2), 2.67–2.60 (t, 4 H, CH_2), 2.56–2.49 (t, 4 H, CH_2), 1.74–1.60 (q, 4 H, CH_2) ppm.

Synthesis of the Iron(II) Complex: $FeCl_2{\cdot}2H_2O$ (24.4 mg, 0.15 mmol) was dissolved in 2 mL of ethanol/methanol (1:1 mixture), and Hpy-DAPP (60.7 mg, 0.15 mmol) in 2 mL of the same mixture of alcohols was added. A light yellow-green solution was formed. The addition of 116.2 mg (0.30 mmol) of NBu_4BF_4 in 4 mL of ethanol/methanol turned the color of this solution to green. The solution was filtered and allowed to stand overnight at room temperature to give green crystals of $[Fe(Hpy\text{-}DAPP)](BF_4)_2$, which were collected by filtration, washed with ethanol, and dried in vacuo. The crystal used in the X-ray structure determination was selected from this sample. $C_{24}H_{32}B_2F_8FeN_6$ (634.01): calcd. C 45.47, H 5.09, Fe 8.81, N 13.26; found C 45.78, H 4.92, Fe 8.52, N 13.01.

Magnetic Properties: Magnetic susceptibilities were measured in the temperature range 15–300 K with a fully automated Manics DSM-10 susceptometer equipped with a TBT continuous-flow cryostat and an electromagnet operating at about 1.6 T. Data were corrected for magnetization of the sample holder and for diamagnetic contributions, which were estimated from the Pascal constants.

Mössbauer Spectra: The variable-temperature ^{57}Fe Mössbauer measurements were carried out on a constant-acceleration spectrometer with a 50 mCi $^{57}Co(Rh)$ source. A powder sample (60 mg) was enclosed in a 12-mm-diameter cylindrical plastic sample holder, the size of which had been determined to optimize the absorption. Spectra were obtained at 5, 100, 150, 200, and 293 K using a custom-designed, liquid helium bath cryostat (DTA, Air Liquid). A second series of measurements was carried out in the 80–250 K range (in the cooling cycle) using a MD306 He exchange gas, liquid nitrogen bath cryostat (Oxford Instruments). A least-squares computer program was used to fit the Mössbauer parameters and to determine the standard deviations of statistical origin (given in parentheses).[19] The isomer shift values are given with respect to metallic iron at room temperature.

Solution and Refinement of the X-ray Structure: The data collection was made with a Nonius Kappa CCD diffractometer equipped with a normal monochromatized focus X-ray tube with a molybdenum target. The selected crystals were mounted on a thin glass fiber. The data were collected using the COLLECT software,[20] then were processed with the DENZO reduction software.[21] Three collections were made: the first one at room temperature (298 K), the second one at 130 K after a slow decrease of the temperature with a cool, dry nitrogen gas stream, and the third one at 90 K after cooling the crystal in a cold nitrogen gas flow. From 10 frames with 1° steps, the initial set of cell parameters was obtained for each measurement. A total of 12331 reflections were collected at room temperature, of which 6326 unique reflections were used for the structure determination. The second collection at 130 K is formed from 10356 measured reflections, 5738 of which were independent reflections. The third collection at 90 K concerns 8580 measured reflections, of which 5358 unique reflections were used for the hypothesis and refinement. The structures were solved by

direct methods with the SHELXS-97 program.[22] The structures were then refined by the least-squares method using SHELXL-97,[23] with anisotropic temperature factors for all non-H atoms. The hydrogen atoms were introduced at calculated positions and refined as riding on their carrier atoms. The final R factor [with $I > 2\sigma(I)$] was 0.059, 0.091, and 0.091 at 298, 130, and 90 K, respectively. Crystal data and refinement results are summarized in Table 4. The perspective view of the asymmetric unit at three temperatures was calculated with PLATON[24] and is shown in Figure 2.

Table 4. Crystallographic data for $[Fe(Hpy\text{-}DAPP)](BF_4)_2$.

	T = 298 K	T = 130 K	T = 90 K
Formula		$C_{24}H_{32}B_2F_8FeN_6$	
Fw	634.03		
a [Å]	13.298(1)	12.897(1)	12.868(1)
b [Å]	14.368(1)	14.251(1)	14.223(1)
c [Å]	15.409(1)	15.207(1)	15.180(1)
β [°]	106.09(1)	106.71(1)	106.69(1)
V [Å^3]	2828.6(1)	2676.9(2)	2661.2(3)
Z	4	4	4
Space group	$P2_1/c$	$P2_1/c$	$P2_1/c$
λ [Å]	0.71073	0.71073	0.71073
$\rho_{calcd.}$ [g cm^{-3}]	1.489	1.573	1.583
μ [cm^{-1}]	6.12	6.47	6.51
R[a] [$I > 2\sigma(I)$]	0.059	0.091	0.091
wR_2[b] [$I > 2\sigma(I)$]	0.141	0.194	0.207

[a] $R = \sum(||F_o| - |F_c||)/\sum|F_o|$. [b] $wR_2 = \{\sum[w(F_o^2 - F_c^2)^2]/\sum[w(F_o^2)^2]\}^{1/2}$.

CCDC-295576 to -295578 contain the supplementary crystallographic data for this paper. These data can be obtained free of charge from The Cambridge Crystallographic Data Center via www.ccdc.cam.ac.uk/data_request/cif.

Electronic Structure Calculations: Calculations of the electronic structure of the isolated $[Fe(Hpy\text{-}DAPP)]^{2+}$ complex cation were performed using the formalism of density functional theory (DFT). Single-point calculations for molecular geometries, extracted from the X-ray crystallographic data for different temperatures, were carried out with the Gaussian 2003 package.[25] In each case, both HS and LS states were considered. The LANL2DZ basis set, including the double-ζ basis with the Los Alamos effective core potential for Fe and the Dunning–Huzinaga all-electron double-ζ basis set with polarization functions for the H, C, and N atoms[26,27] were used. The choice of exchange-correlation functional for calculations of the energy gap between HS and LS states is widely debated in the literature. The hybrid Hartree–Fock/GGA (generalized gradient approximation) B3LYP functional and its re-parameterized version B3LYP* are more often recommended.[28–30] In this work we firstly use the parameter-free density functional model PBE0 obtained by combining the so-called PBE GGA functional with a predefined amount of exact exchange.[31] The calculations with this functional result in a correct order of the HS and LS states for experimental structures obtained at different temperatures.

[1] a) H. A. Goodwin, *Coord. Chem. Rev.* **1976**, *18*, 293; b) J. Zarembowitch, O. Kahn, *New J. Chem.* **1991**, *15*, 181; c) E. König, *Struct. Bond.* **1991**, *76*, 51; d) P. Gütlich, A. Hauser, H. Spiering, *Angew. Chem. Int. Ed. Engl.* **1994**, *33*, 2024; e) O. Kahn, *Molecular Magnetism*; VCH Publishers, New York, **1993**; f) J. A. Real, *Transition Metals in Supramolecular Chemistry* (Ed.: J. P. Sauvage), John Wiley & Sons, **1999**; g) M. Sorai, *Bull. Chem. Soc. Jpn.* **2001**, *74*, 2223; h) *Topics in Current Chemistry*, vol. 233–235, *Spin Crossover in Transition Metal Compounds I–III* (Eds.: P. Gütlich, H. A. Goodwin), Springer, Berlin, **2004**; i) A. Bousseksou, G. Molnár, G. S. Matouzenko, *Eur. J. Inorg. Chem.* **2004**, 4353; j) J. A. Real, A. B. Gaspar, V. Niel, M. C. Muñoz, *Coord. Chem. Rev.* **2003**, *236*, 121; k) J. A. Real, A. B. Gaspar, M. C. Muñoz, *Dalton Trans.* **2005**, 2062.

[2] a) O. Kahn, J. P. Launay, *Chemtronics* **1988**, *3*, 140; b) O. Kahn, J. Kröber, C. Jay, *Adv. Mater.* **1992**, *4*, 718; c) A. Bousseksou, G. Molnár, P. Demont, J. Menegotto, *J. Mater. Chem.* **2003**, *13*, 2069.

[3] a) O. Kahn, E. Codjovi, *Philos. Trans. R. Soc. London, Ser. A* **1996**, *354*, 359; b) O. Kahn, Y. Garcia, J. F. Létard, C. Mathonière, *NATO ASI Ser., Ser. C* **1998**, *518*, 127.

[4] a) G. S. Matouzenko, A. Bousseksou, S. Lecocq, P. J. van Koningsbruggen, M. Perrin, O. Kahn, A. Collet, *Inorg. Chem.* **1997**, *36*, 2975; b) G. S. Matouzenko, A. Bousseksou, S. Lecocq, P. J. van Koningsbruggen, M. Perrin, O. Kahn, A. Collet, *Inorg. Chem.* **1997**, *36*, 5869.

[5] D. Cremer, J. A. Pople, *J. Am. Chem. Soc.* **1975**, *97*, 1354.

[6] G. S. Matouzenko, A. Bousseksou, S. A. Borshch, M. Perrin, S. Zein, L. Salmon, G. Molnár, S. Lecocq, *Inorg. Chem.* **2004**, *43*, 227.

[7] N. N. Greenwood, T. C. Gibb, *Mössbauer Spectroscopy*, Chapman and Hall Ltd., London, UK, **1971**.

[8] a) J. A. Real, H. Bolvin, A. Bousseksou, A. Dworkin, O. Kahn, F. Varret, J. Zarembowitch, *J. Am. Chem. Soc.* **1992**, *114*, 4650; b) J. A. Real, I. Castro, A. Bousseksou, M. Verdaguer, R. Burriel, M. Castro, J. Linares, F. Varret, *Inorg. Chem.* **1997**, *36*, 455.

[9] a) Y. Garcia, O. Kahn, L. Rabardel, B. Chansou, L. Salmon, J.-P. Tuchagues, *Inorg. Chem.* **1999**, *38*, 4663; b) G. S. Matouzenko, J.-F. Létard, A. Bousseksou, S. Lecocq, L. Capes, L. Salmon, M. Perrin, O. Kahn, A. Collet, *Eur. J. Inorg. Chem.* **2001**, *11*, 2935; c) W. Hibbs, P. J. van Koningsbruggen, A. M. Arif, W. W. Shum, J. S. Miller, *Inorg. Chem.* **2003**, *42*, 5645.

[10] a) D. Boinnard, A. Bousseksou, A. Dworkin, J. M. Savariault, F. Varret, J.-P. Tuchagues, *Inorg. Chem.* **1994**, *33*, 271; b) D. Chernyshov, M. Hostettler, K. W. Törnroos, H.-B. Bürgi, *Angew. Chem. Int. Ed.* **2003**, *42*, 3825.

[11] G. A. Renovitch, W. A. Baker Jr., *J. Am. Chem. Soc.* **1967**, *89*, 6377.

[12] a) M. Mikami, M. Konno, Y. Saito, *Chem. Phys. Lett.* **1979**, *63*, 566; b) B. A. Katz, C. E. Strouse, *J. Am. Chem. Soc.* **1979**, *101*, 6214; c) M. Mikami, M. Konno, Y. Saito, *Acta Crystallogr., Sect. B* **1980**, *36*, 275.

[13] a) H. Köppen, E. W. Müller, C. P. Köhler, H. Spiering, E. Meissner, P. Gütlich, *Chem. Phys. Lett.* **1982**, *91*, 348; b) K. Kaji, M. Sorai, *Thermochim. Acta* **1985**, *88*, 185.

[14] a) R. Jakobi, H. Spiering, P. Gütlich, *J. Phys. Chem. Solids* **1992**, *53*, 267; b) H. Romstedt, H. Spiering, P. Gütlich, *J. Phys. Chem. Solids* **1998**, *59*, 1253; c) H. Spiering, T. Kohlhaas, A. Hauser, C. Bruns-Yilmaz, J. Kusz, P. Gütlich, *Coord. Chem. Rev.* **1999**, *190–192*, 629; d) J. Kusz, D. Schollmeyer, H. Spiering, P. Gütlich, *J. Appl. Crystallogr.* **2005**, *38*, 528.

[15] P. Poganiuch, S. Decurtins, P. Gütlich, *J. Am. Chem. Soc.* **1990**, *112*, 3270.

[16] a) S. Alvarez, *J. Am. Chem. Soc.* **2000**, *125*, 6795; b) *Topics in Current Chemistry*, vol. 234, *Spin Crossover in Transition Metal Compounds I–III* (Eds.: P. Gütlich, H. A. Goodwin), Springer, Berlin, **2004**, p. 98; c) M. Marchivie, P. Guionneau, J.-F. Létard, D. Chasseau, *Acta Crystallogr., Sect. B* **2005**, *61*, 25.

[17] a) M. Sorai, *Bull. Chem. Soc. Jpn.* **2001**, *74*, 2223; b) M. Sorai, *J. Chem. Thermodyn.* **2002**, *34*, 1207; c) M. Sorai, *Pure Appl. Chem.* **2005**, *77*, 1331.

[18] H. R. Chang, J. K. McCusker, H. Toftlund, S. R. Wilson, A. X. Trautwein, H. Winkler, D. N. Hendrickson, *J. Am. Chem. Soc.* **1990**, *112*, 6814.

[19] F. Varret, *Proceedings of the International Conference on Mössbauer Effect Applications*, Jaipar, India, **1981**; Indian National Science Academy, New Delhi, **1982**.

[20] Nonius, *COLLECT*, Nonius BV, Delf, The Netherlands, **1997–2000**.

[21] Z. Otwinowski, W. Minor, *Methods Enzymol.* **1997**, *276*, 307.
[22] G. M. Sheldrick, *SHELXS-97*, *Program for Crystal Structure Determination*; University of Göttingen, Germany, **1997**.
[23] G. M. Sheldrick, *SHELXL-97*, *Program for Crystal Structure Refinement*; University of Göttingen, Germany, **1997**.
[24] A. L. Spek, *PLATON, A Multipurpose Crystallographic Tool*; Utrecht University, Utrecht, The Netherlands, **1999**.
[25] M. J. Frisch, G. W. Trucks, H. B. Schlegel, G. E. Scuseria, M. A. Robb, J. R. Cheeseman, J. A. Montgomery Jr., T. Vreven, K. N. Kudin, J. C. Burant, J. M. Millam, S. S. Iyengar, J. Tomasi, V. Barone, B. Mennucci, M. Cossi, G. Scalmani, N. Rega, G. A. Petersson, H. Nakatsuji, M. Hada, M. Ehara, K. Toyota, R. Fukuda, J. Hasegawa, M. Ishida, T. Nakajima, Y. Honda, O. Kitao, H. Nakai, M. Klene, X. Li, J. E. Knox, H. P. Hratchian, J. B. Cross, V. Bakken, C. Adamo, J. Jaramillo, R. Gomperts, R. E. Stratmann, O. Yazyev, A. J. Austin, R. Cammi, C. Pomelli, J. W. Ochterski, P. Y. Ayala, K. Morokuma, G. A. Voth, P. Salvador, J. J. Dannenberg, V. G. Zakrzewski, S. Dapprich, A. D. Daniels, M. C. Strain, O. Farkas, D. K. Malick, A. D. Rabuck, K. Raghavachari, J. B. Foresman, J. V. Ortiz, Q. Cui, A. G. Baboul, S. Clifford, J. Cioslowski, B. B. Stefanov, G. Liu, A. Liashenko, P. Piskorz, I. Komaromi, R. L. Martin, D. J. Fox, T. Keith, M. A. Al-Laham, C. Y. Peng, A. Nanayakkara, M. Challacombe, P. M. W. Gill, B. Johnson, W. Chen, M. W. Wong, C. Gonzalez, and J. A. Pople, *Gaussian 03*, Revision C.02, Gaussian, Inc., Wallingford CT, **2004**.
[26] T. H. Dunning Jr., P. J. Hay, *Modern Theoretical Chemistry* (Ed.: H. F. Schaefer III), vol. 3, Plenum, New York, **1976**, p. 1–28.
[27] P. J. Hay, W. R. Wadt, *J. Chem. Phys.* **1985**, *82*, 270.
[28] a) S. Zein, G. S. Matouzenko, S. A. Borshch, *J. Phys. Chem. A* **2005**, *109*, 8568; b) S. Zein, S. A. Borshch, *J. Am. Chem. Soc.* **2005**, *127*, 16197; c) S. Zein, G. S. Matouzenko, S. A. Borshch, *Chem. Phys. Lett.* **2004**, *397*, 475.
[29] G. Brehm, M. Reiher, S. Schneider, *J. Phys. Chem. A* **2002**, *106*, 12024.
[30] M. Reiher, *Inorg. Chem.* **2002**, *41*, 6928.
[31] C. Adamo, V. Barone, *J. Chem. Phys.* **1999**, *110*, 6158.

Received: January 23, 2006
Published Online: April 25, 2006

